EXPERIMENTAL EXAMINATION OF GUST EFFECT FACTORS OF WIND LOADS ON LOW-RISE BUILDING ROOFS

Jigar Mokani[1][0000-0002-9810-3555] and Jin Wang[2] [0000-0001-9536-6432]

[1]M.E.Sc. student, Department of Civil & Environment Engineering, University of Western Ontario, Canada, N6A 5B9

[2]Assistant professor, Department of Civil & Environment Engineering, University of Western Ontario, Canada, N6A 5B9; jwan2225@uwo.ca

Abstract. The traditional approach for predicting wind loads on the components and cladding (C&C) of roofs in low-rise buildings involves using directly measured peak wind pressure coefficients obtained from wind tunnel testing, as outlined in ASCE 7-22 and NBCC 2020. However, the Euro-code (EN 1991-14) recommends a constant gust effect factor of 1.0 for C&C wind loads, implicitly the negligible body-generated turbulence effects. This study aims to evaluate the gust effect factors of wind loads on C&C by analyzing their statistical properties. The research utilizes aerodynamic data from the NIST database, obtained from the Boundary-Layer Wind Tunnel II at the University of Western Ontario. The focus is on four specific low-rise building configurations with varying roof heights. The analysis includes an exploration of statistical properties, such as mean, standard deviation, skewness, kurtosis, and peak factor of wind load coefficients, considering varying tributary areas and zone locations. In addition, this study assesses the background response factor, which reflects the relationship between wind load fluctuation and upstream turbulence. The findings reveal non-Gaussian features of wind loads in the corner and edge regions of roofs, due to the body-generated turbulence, leading to gust effect factors scattered around 1.5 for C&C wind loads of these regions.

Keywords: low-rise buildings, components and cladding, gust effect factor, quasi-steady theory

1 Introduction

Significant damage has been observed on low-rise buildings' roofs under windstorms, due to the flow separation within these regions [1]. These damages are mostly related to the components and claddings (C&C) of roofs, which consist of roof supporting members, shingles, underlayment felts and sheathing [2]. Therefore, accurately prediction of wind loads on buildings' roofs are essential in the safety and serviceability design of these structures.

Wind-induced loadings on structures can be estimated by mainly two methods. The first approach utilizes directly measured instantaneous peak wind pressure coefficients

obtained from wind tunnel testing. The second method refers to gust effect factor method, which is used to assess the peak structural response of high-rise buildings in the along-wind direction. The latter method was initially proposed by Davenport [3], named as gust response factor, which is the ratio of extreme structural response to the mean response. Solari [4, 5] related the peak structural response to the gust wind speed and proposed the concept of gust effect factor. The development of gust effect factor is based on quasi-steady theory (QST), which assumes that the fluctuations of wind load and structural response are linearly related to the upstream turbulence. Based on QST, a Gaussian distribution is further assumed for both wind-induced loadings and structural response, since the wind velocity is commonly assumed to follow Gaussian distribution. Therefore, the explicit indication of gust effect factor method is the negligible body-generated turbulence effects [4, 5]. With regard to low-rise buildings' roofs, the classical QST is not applicable due to the flow separation at the sharp edge [6]. However, Wu and Kopp [7] conclude that QST's performance for predicting roofs' uplift is still acceptable by adopting the quasi-steady-vector model, which considers the horizontal azimuth and vertical elevation angles. Wang and Kopp [8] further examine the gust effect factors for overall uplift for buildings ranging from low- to high-rise. The authors argued that statistical properties of roof uplift depend on the ratio of building height to the roof length in the along-wind direction. Uplift on longer roof with flow reattachment is tending to possess more Gaussian characteristics.

For C&C of building envelops, both methods have been advocated in the various building codes. ASCE 7-22 [9] employs the first method (directly measured peak pressure coefficients) to estimate wind-induced loadings on C&C of buildings. NBCC 2020 [10] recommends the use of the first method for C&C of low-rise buildings with height less than 20m, and the second method for high buildings with roof height exceeding 20m. EN1991-1-4 [11] offers provisions based on the gust effect factor framework for C&C of buildings. It deserves noting that NBCC 2020 and EN1991-1-4 provide a constant gust effect factor of 2.5 and 1.0, respectively for C&C. This discrepancy arises from differences in the reference wind speed. In addition, ASCE 7-22 provides a constant gust effect factor of 0.85 for estimating wind-induced loading on the rigid main wind force resisting system (MWFRS). However, there is a lack of research on the examination of gust effect factors of C&C of low-rise buildings, which motivates the present study. Additionally, the construction of long-span roof structures coupled with lightly weighted façade elements may escalate the dynamic effects of low-rise structures. Unfortunately, the existing prevailing code provisions do not consider the dynamic effects of C&C. Therefore, it is also essential to assess the gust effect factors of C&C by separating the background and resonant response effects.

The objective of this research is to examine the gust effect factors of C&C for low-rise buildings' roofs. The present study mainly focuses on low-sloped gable roofs ($\leq$ 7°) of low-rise buildings. The aerodynamic database in National Institute of Standards and Technology (NIST), obtained from Boundary-Layer Wind Tunnel testing at the University of Western Ontario, is employed. Section 2 describes the methodology. Section 3 exhibits the analysis results. Section 4 concludes the study.

2 Methodology

This section describes the experimental datasets for the selected buildings, and adopted statistical parameters. Additionally, a brief description on the procedure for varying non-overlapping tributary areas on the roof is provided.

2.1 Aerodynamic database

Four buildings from NIST database [12] were selected for this study. The geometrical information of these buildings is shown in Table 1 and Fig. 1. The wind tunnel tests were carried on each of the selected buildings with respect to 37 different wind directions ranging from 180° to 360° with the increment of 5° [12]. During the experiment, the adopted length scale was 1:100 and the velocity scale was 1:4 with respect to full-scale model and target wind speed, respectively. In this study, only experimental results between the wind directions of 270° to 360° were used to calculate the wind loads for regions with high resolution of pressure taps, as shown in Fig. 2. The wind pressures were measured with the sampling frequency of 500 Hz for 100 s sampling period. Wind tunnel speed at reference height was measured at 45 ft/s, which could be interpreted as 84 mph with an equivalent 22 samples per second for 0.64 min in full scale in open terrain.

Table 1. Building geometries (full-scale) from NIST database

No	Model No.	Roof slope (tan)	Roof slope (°)	Length L (ft)	Width W (ft)	Eave height H (ft)	H/B	H/L
1	M2-16	1:12	4.76	125	80	16	0.20	0.13
2	M2-24	1:12	4.76	125	80	24	0.30	0.19
3	M2-32	1:12	4.76	125	80	32	0.40	0.26
4	M2-40	1:12	4.76	125	80	40	0.50	0.32

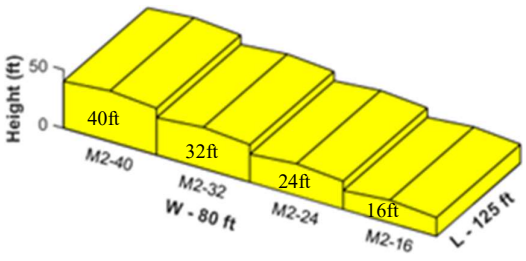

Fig. 1. Building configurations considered in this study

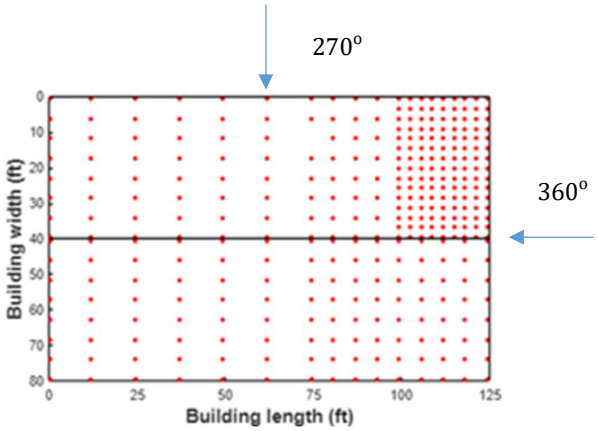

Fig. 2. Pressure tap layouts on building roof

2.2 Area-averaged wind pressures on varying tributary areas

In this research, the statistics of area-averaged wind pressures on varying tributary areas are exhibited, along with gust effect factor. The method outlined in [13] was employed to define the non-overlapping tributary area on the roof. Given the varying density of pressure taps, a mesh of taps with a spacing of 1'×1' was used. The assignment of wind pressure time history to the selected mesh point was carried out based on the nearest pressure tap. The minimum tributary area is 9 ft^2 (3'×3'), incrementally increasing by 1' from two adjacent sides of each pixel. Hence, subsequent tributary areas are 16 ft^2, 25 ft^2, and so forth, gradually increasing till the maximum size reaching to the half of the building width. While the mentioned statistical parameters were estimated for all 19 wind directions, only the statistical results corresponding to the worst peak pressure coefficients have been shown in Section 3.

2.3 Estimation of statistical parameters

The statistical peaks were estimated by dividing time histories (series of instantaneous pressure results) into 16 segments. The peaks from each segment were extracted and then fitted to the Gumbel distribution using Leiblein best linear unbiased estimator (BLUE) method at 78^{th} percentile. The estimated peaks from Gumbel distribution were extrapolated to those within 1 h at full scale based on the method outlined in Cook and Mayne [14].

This study particularly focuses on mean, standard deviation, skewness, kurtosis, peak factor and background response factor of wind pressures. Skewness and kurtosis provide the indication of Gaussian and non-Gaussian distribution. While background response factor indicate the relationship between wind pressure fluctuation and up-stream turbulence. The definitions of these parameters can be found in Wang and Kopp [8], which are not repeated herein.

3 Results and discussion

In this section, results related to two building models (M2-16 and M2-40) have been shown with respect to specific tributary areas (i.e., 9 ft^2 and 100 ft^2) to illustrate the effects of building height and tributary area, respectively. In addition, gust effect factors versus varying tributary areas for three zones on the roof have been shown for all four selected buildings. Note that the zones are demarcated as per the definitions given in 4.1.7.6-C of NBCC 2020, as shown in Fig. 3.

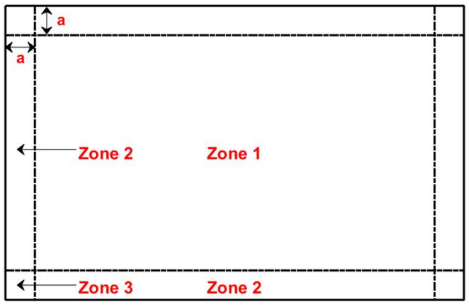

Fig. 3. Zone demarcation of low-sloped roof on low-rise buildings in NBCC 2020

3.1 Distribution of mean and standard deviation of pressure coefficients

Fig. 4 shows the magnitude of mean pressure coefficients on the selected two buildings. Higher mean pressure coefficient (more negative) is observed at the corner region (Zone 3), which is consistent with the findings of [13]. The magnitude of mean pressure reduces as the distance increases from the windward edge. Moreover, as the tributary area increases from 9 ft^2 to 100 ft^2, the overall magnitude of mean pressure coefficient reduces due to the dilution of area-averaged pressures. Furthermore, the magnitude of pressure coefficient increases with building height. Among all cases, the maximum mean pressure coefficient has been observed at corner region, which is caused by the conical vortices, and their effects increase with the building height [1].

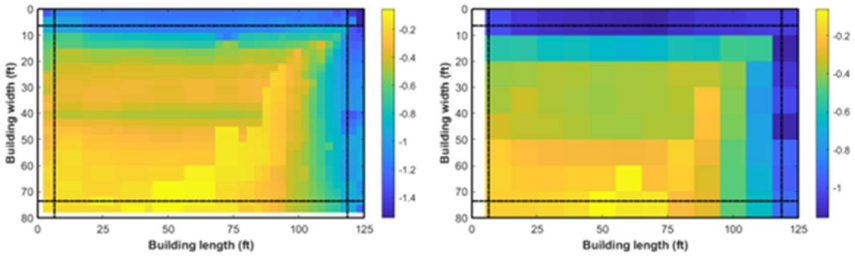

(a) (b)

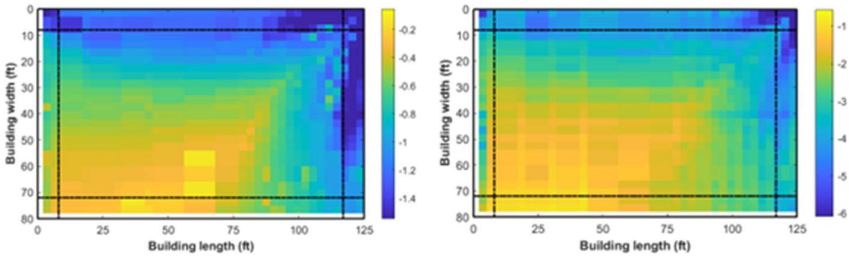

Fig. 4. Spatial plots for mean pressure coefficient for varying tributary areas: (a) M2-16 – 9 ft^2, (b) M2-16 – 100 ft^2, (c) M2-40 – 9 ft^2 and (d) M2-40 – 100 ft^2

Standard deviation of pressure coefficients is shown in Fig. . The trend of these values is similar with that of mean pressure coefficient. It is worth highlighting that the magnitude of standard deviation increases as the building height increases. This might be caused by the increment in the size of separation bubble resulting in higher fluctuations of wind pressures [1]. Moreover, area-averaging effects reduce the overall magnitude of values, and this phenomenon has been observed in all statistical parameters.

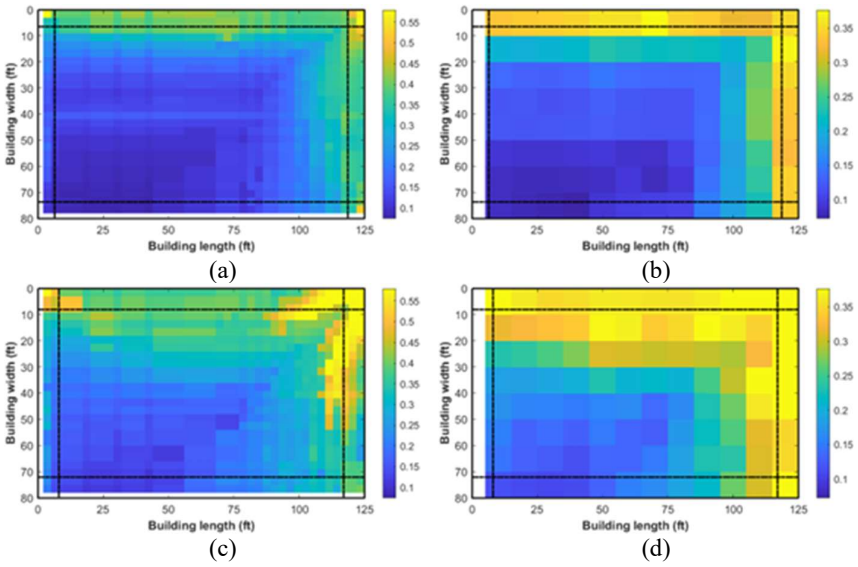

Fig. 5. Spatial plots in varying effective wind area for standard deviation: (a) M2-16 – 9 ft^2, (b) M2-16 – 100 ft^2, (c) M2-40 – 9 ft^2 and (d) M2-40 – 100 ft^2

3.2 Skewness and Kurtosis

Fig. 6 shows the results related to skewness for building M2-40 with two different tributary areas, i.e., 9ft^2 and 100ft^2. The trend of magnitude is as similar as the trend of mean pressure coefficient. A higher magnitude has been observed at corner region due to the strong coherent conical vortices. Hence, it can be concluded that wind loads at windward edges and corners have highly non-Gaussian features, which is consistent with findings in [8, 15].

Fig. shows the kurtosis values for building M2-40. Compared with skewness distribution, the kurtosis of wind pressure coefficients are much more scattered over the entire roof. Overall, the skewness and kurtosis results show that the wind loads on corner regions have non-Gaussian characteristics.

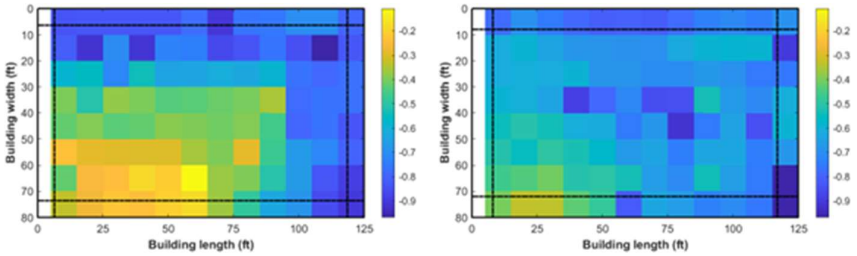

Fig. 6. Spatial plots for skewness: (a) M2-40 – 9 ft^2 and (b) M2-40 – 100 ft^2

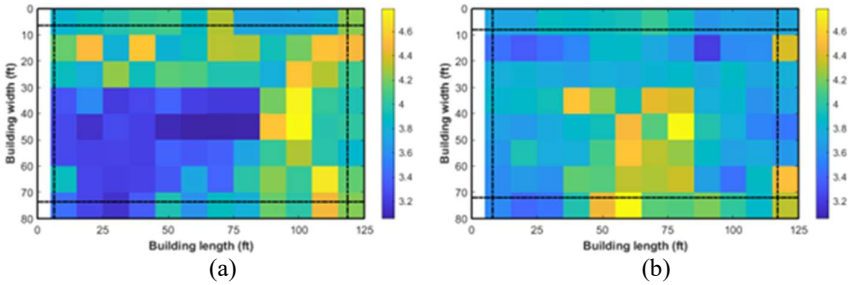

Fig. 7. Spatial plots for kurtosis: (a) M2-40 – 9 ft^2 and (b) M2-40 – 100 ft^2

3.3 Peak factor

Fig. 8 provides the results related to the peak factors of wind pressure coefficients for building M2-40. The contour of the data shows scatteredness across the entire roof. The derived peak factors are much higher than the recommended value of 3.4 for Gaussian distribution by Solari [4, 5]. This observation implicitly indicates that the existing gust effect factor model with assumption of Gaussian distribution might underestimate the wind-induced loading for C&C.

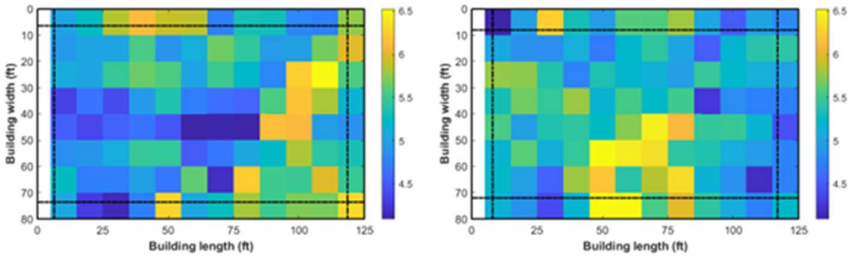

(a) (b)

Fig. 8. Spatial plots for peak factor: (a) M2-40 – 9 ft^2 and (b) M2-40 – 100 ft^2

3.4 Background response factor

Background response factor is a dimensionless parameter that characterizes the connection between wind load fluctuation and the upstream turbulence. Its unit indicates the linear correlation between the upstream turbulence and wind load fluctuation. Conversely, a background reground response factor greater than one implies that the body-generated turbulence could influence wind load fluctuation. Therefore, it is highly related to the application of gust effect factor framework. The background response factor of unit indicates that the fluctuation of wind pressure is fully related to the upstream turbulence. Fig. 9 shows the results concerning the background response factor for building M2-40. The magnitudes of background response factors are scattered over Zones 3 and 2. In addition, it is interesting to observe increased background response factor for the inner zone, i.e., Zone 1. The reduced mean pressure coefficients for Zone 1 is responsible for this phenomenal. Overall, the measured background response factors exceed the value of unit, due to the body-generated turbulence effects.

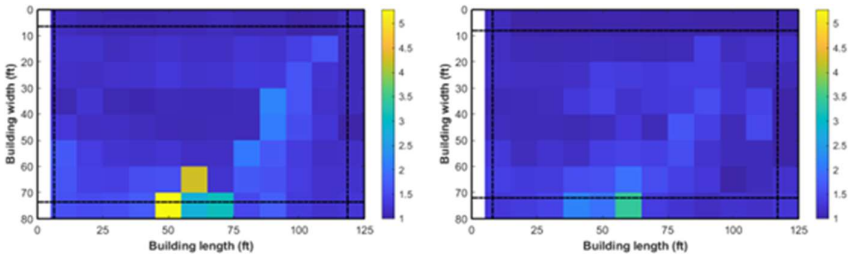

(a) (b)

Fig. 9. Spatial plots for background response factor: (a) M2-40 – 9 ft^2 and (b) M2-40 – 100 ft^2

3.5 Peak external pressure coefficient ($C_g C_p$)

Fig. 10 shows the contours for peak external pressure coefficients in format of $C_g C_p$, as provided in NBCC 2020. The tendency of the derived values is similar to that for other statistical properties. There, we will not repeat the description for brevity.

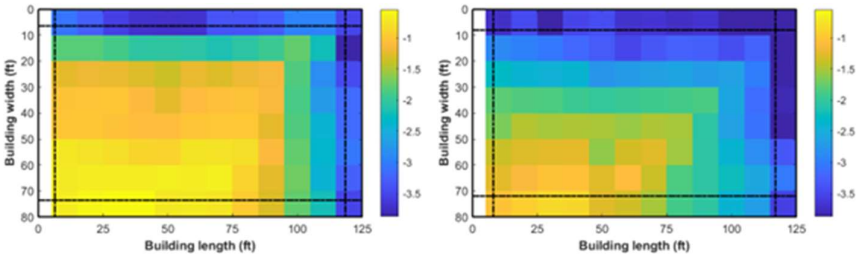

Fig. 10. Spatial plots for peak external pressure coefficient: (a) M2-40 – 9 ft^2 and (b) M2-40 – 100 ft^2

3.6 Gust effect factors for varying tributary areas

Fig. 11 shows the gust effect factors (G) versus varying tributary areas for the three specific zones, i.e., Zones 1, 2 and 3. The results for four buildings with different heights are included in Fig. 11. For corner zone (Zone 3) as shown in Fig. 11 (a), the gust effect factors are scattered around 1.5 with varying tributary areas for all considered buildings. The same observation is found for the edge zone (Zone 2), as shown in Fig. 11 (b). However, it is interesting to find the gust effect factors for building with roof height of 40 ft are higher than those for low buildings. The same observation is found in the statistical characteristics of wind pressure coefficients as discussed in the preceding sections. Moreover, it is worth noting that the derived gust effect factors are considerably higher than the recommended value of 1.0 as per EN 1991-1-4, which indicates that the recommended value without consideration of body-generated turbulence would underestimate the wind-induced pressures for C&C of roofs. For inner zone (Zone 1), the derived gust effect factors show a reduced tendency with tributary area. However, for tributary areas less than 250 ft^2, the gust effect factors are scattered around 1.5.

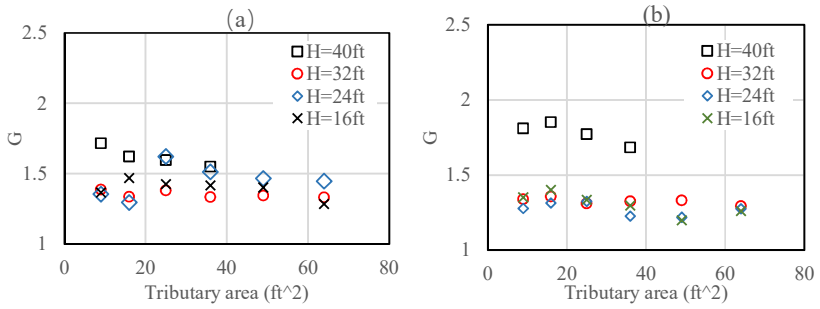

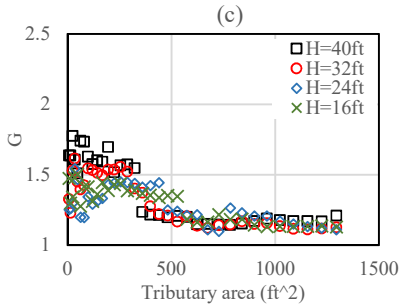

Fig. 11. Gust effect factors versus varying tributary areas for: (a) Zone 3 and (b) Zone 2; and (c) Zone 1.

4 Conclusion

This study aims to assess the gust effect factors of area-averaged wind loads for C&C of low-rise building roofs. Wind pressure data from the NIST aerodynamic database is utilized in this study. In order to illustrate the effects of body-generated turbulence on statistical features of wind loads, the peak factor of wind pressure, background response factor, skewness and kurtosis were examined in detail with respect to varying tributary areas. The derived gust effect factors are compared with the given values in EN 1991-1-4. The conclusions of this study are as follows:

1) Separated shear layers and conical vortices are responsible for peak wind pressures at windward edges and corners of roofs. The distribution of statistical parameters, such as skewness and kurtosis of wind pressures, indicates that wind loads have more non-Gaussian features at corner and edge regions of roofs.

2) The peak factor and background response factor of wind pressure are scattered across the roof, especially at corner and edge regions. The background response factors at inner zone are higher than those in the corner and edge regions, due to the reduced mean pressure coefficients.

3) The derived value for gust effect factor (G) is greater than the recommended value of 1.0 in EN 1991-1-4, due to the negligible body-generated turbulence effects. When incorporating the gust effect factor concept into the design of C&C, it is crucial to account for the body-generated turbulence effects to accurately estimate the peak wind loads on roof elements.

The conclusions in this study will be further examined for the remaining buildings in NIST database. The building geometry effects on gust effect factors for C&C will be considered afterwards.

5 Acknowledgement

The authors gratefully acknowledge Start-up Grant and WSS-Seed Grants awarded by University of Western Ontario, and NSERC Discovery Grant.

6 References

[1] Akon, A.F. and Kopp, G.A., 2016. Mean pressure distributions and reattachment lengths for roof-separation bubbles on low-rise buildings. *Journal of Wind Engineering and Industrial Aerodynamics*, *155*, pp.115-125.

[2] He, J., Pan, F. and Cai, C.S., 2018. Assessment of ASCE 7-10 for wind effects on low-rise wood frame buildings with database-assisted design methodology. *Wind Struct*, *27*(3), pp.163-173.

[3] Davenport, A.G., 1964. Note on the distribution of the largest value of a random function with application to gust loading. *Proceedings of the Institution of Civil Engineers*, *28*(2), pp.187-196.

[4] Solari, G., 1993. Gust buffeting. I: Peak wind velocity and equivalent pressure. *Journal of Structural Engineering*, *119*(2), pp.365-382.

[5] Solari, G., 1993. Gust buffeting. II: Dynamic alongwind response. *Journal of Structural Engineering*, *119*(2), pp.383-398.

[6] Banks, D. and Meroney, R.N., 2001. The applicability of quasi-steady theory to pressure statistics beneath roof-top vortices. *Journal of Wind Engineering and Industrial Aerodynamics*, *89*(6), pp.569-598.

[7] Wu, C.H. and Kopp, G.A., 2018. A quasi-steady model to account for the effects of upstream turbulence characteristics on pressure fluctuations on a low-rise building. *Journal of Wind Engineering and Industrial Aerodynamics*, *179*, pp.338-357.

[8] Wang, J. and Kopp, G.A., 2023. Gust effect factors for regions of separated flow around rigid low-, mid-, and high-rise buildings. *Journal of Wind Engineering and Industrial Aerodynamics*, *232*, p.105254.

[9] ASCE, 2022. Minimum design loads for buildings and other structures. ASCE 7-22, Reston, VA.

[10] National Building Code of Canada (NBC), 2020. National Building Code of Canada 2020.

[11] EN 1991-1-4, 2005. Eurocode 1: Actions on Structures—Part 1–4: General Actions—Wind Actions. Brussels (Belgium): Comité Européen de Normalization (CEN).

[12] Ho, T.E., Surry, D., Morrish, D. and Kopp, G.A., 2005. The UWO contribution to the NIST aerodynamic database for wind loads on low buildings: Part 1. Archiving format and basic aerodynamic data. *Journal of Wind Engineering and Industrial Aerodynamics*, *93*(1), pp.1-30.

[13] Kopp, G.A. and Morrison, M.J., 2018. Component and cladding wind loads for low-slope roofs on low-rise buildings. *Journal of Structural Engineering*, *144*(4), p.04018019.

[14] Cook, N.J. and Mayne, J.R., 1981. A novel working approach to the assessment of wind loads for equivalent static design a refined working approach to the assessment of wind loads for equivalent static design. *Journal of Wind Engineering and Industrial Aerodynamics*, *8*(3), pp.299-301.

[15] Holmes, J.D., 1981. Non-Gaussian characteristics of wind pressure fluctuations.